2D CFD Analysis of Servovalve Main Stage Internal Leakage

Conference Paper · October 2019

DOI: 10.1115/FPMC2019-1705

8 authors, including:

Paolo Tamburrano
Politecnico di Bari
55 PUBLICATIONS **655** CITATIONS
SEE PROFILE

Andrew R. Plummer
University of Bath
132 PUBLICATIONS **2,028** CITATIONS
SEE PROFILE

Elia Distaso
Politecnico di Bari
47 PUBLICATIONS **500** CITATIONS
SEE PROFILE

Riccardo Amirante
Politecnico di Bari
120 PUBLICATIONS **1,256** CITATIONS
SEE PROFILE

Proceedings of the ASME/BATH 2019
Symposium on Fluid Power and Motion Control
FPMC2019
October 7-9, 2019, Longboat Key, FL, USA

FPMC2019-1705

2D CFD ANALYSIS OF SERVOVALVE MAIN STAGE INTERNAL LEAKAGE

Paolo Tamburrano
Centre for PTMC, University of Bath, Bath, UK;
& DMMM, Polytechnic University of Bari, Bari, Italy
(corresp. author: paolo.tamburrano@poliba.it)

Andrew R. Plummer
Centre for power transmission and motion control (PTMC), University of Bath, Bath, UK

Phil Elliott
Moog Controls Ltd, Aircraft Group, Tewkesbury, UK

William Morris
Moog Controls Ltd, Aircraft Group, Tewkesbury, UK

Sam Page
Moog Controls Ltd, Aircraft Group, Tewkesbury, UK

Elia Distaso
Department of Mechanics, mathematics and management (DMMM), Polytechnic University of Bari, Bari, Italy

Riccardo Amirante
Department of Mechanics, mathematics and management (DMMM), Polytechnic University of Bari, Bari, Italy

Pietro De Palma
Department of Mechanics, mathematics and management (DMMM), Polytechnic University of Bari, Bari, Italy

ABSTRACT

This paper presents research aimed at understanding the effects of geometrical imperfections and tolerances upon the internal leakage occurring around null in the main stages of servovalves. Specifically, a two-dimensional (2D) computational fluid dynamic analysis was used to predict the direct leakage flow as a function of the overlap and clearance between the spool and bushing sleeve, as well as the roundness on the edges of the spool and bushing sleeve. Predictions of direct leakage flow against edge overlap, which have general validity, are provided in the paper for three selected values of the pressure drop. For different values of the pressure drop, analytical correlations can be applied using the data retrieved from these graphs. The analysis shows that the leakage flow is highly affected by the above-mentioned geometrical parameters. As expected, for given values of overlap and radial clearance, the greater the roundness of the edges caused by manufacturing processes or wear, the higher the leakage flow. For low leakage and hence low power loss requirement, the radii on the spool and bushing sleeve as well as the clearance must be maintained as low as possible. In addition, it is well-known that overlap between the spool and its bushing sleeve can help to reduce the leakage flow at null, and the effect of edge roundness on this reduction is now revealed.
Keywords: servovalve, leakage, roundness, clearance, CFD

INTRODUCTION

The internal leakage occurring in servovalves is a significant feature of these valves. In some systems it is required for cooling, and in others it causes unwanted power consumption during operation. The overall internal leakage is the sum of two contributions: the leakage occurring in the pilot stage and the leakage occurring in the main stage [1]. While the leakage in the pilot stage is almost constant regardless of the spool position, the leakage in the main stage is negligible at large openings but increases with decreasing spool position, being maximum at null. This causes the internal leakage to be maximum when the system driven by the valve is at rest [2].

Because of its great importance to the performance of a servovalve, the leakage around null in the main stage has been predicted in the scientific literature through analytical models. Merritt derived an equation which is valid for a four-way three-position (4/3) critically centered valve (namely, with zero overlap between the spool lands and the bushing edges), having sharp edges of the spool and the bushing. This equation, which assumes that the flow is laminar, allows the overall leakage to be calculated at null with blocked load ports, as follows [3]:

$$Q_c = \frac{\pi c^2 w}{32\mu} p_s \tag{1}$$

where c is the clearance between spool and bushing, w is the slot width, μ is the dynamic viscosity and p_s the supply pressure.
However, this equation is not capable of taking into account real conditions, such as the overlap (or underlap, less common) which is usually present in servovalves, despite being very small. In addition, real valves present geometrical imperfections, and a radius can exist on the edges of both the spool and the bushing because of manufacturing processes. In fact, after a spool and its bushing sleeve have been constructed, in order to achieve a precise overlap between the spool lands and the slots of the bushing sleeve, a grinding process is performed on the faces. However, this process usually leads to the formation of undesired burrs, namely unwanted pieces of material attached to the edge. These irregularities need to be removed through a process, which is usually manual, called deburring. The main drawback stemming from this process is that the sharp edges can be rounded with a small radius; despite being very small, this micro radius can change the spool valve null region characteristics, which have an important influence on the valve performance. Moreover, the presence of contamination particles in the hydraulic oil can wear the edges, thus increasing the radius of the edges.
In the scientific literature there are some analytical models which try to improve equation 1 by taking into account geometrical imperfections and some degree of overlap between the spool land width and the port width of the bushing sleeve. These are commonly semi-empirical equations which require experimental parameters to be found to be applied to existing servovalves [4-7]. An extensive comparison among the available analytical models and experimental data was performed in [5]. According to those authors [5], their model provides better results compared to the other ones; however, the difference between the predictions of all the analytical models and the experimental data seems to be very high for overlap conditions.
This is due to the fact that it is very difficult to evaluate, through analytical models, the effects of the edge conditions upon the internal leakage. Instead, the use of computational fluid dynamics (CFD) can be instrumental in obtaining accurate predictions of the internal leakage, assessing the effects of real edge conditions, such as the presence of radii on the edges, radial clearance between the spool and the bushing sleeve, and some degree of overlap. Some papers present in the scientific literature prove that the use of CFD to study the internal leakage can be viable. In [8], a partial 3D model was developed in the STAR-CD environment to analyze the flow through a commercially available servovalve (Moog D633 servovalve). The objective of that study was to predict the values of the discharge coefficients in the metering sections, for different opening degrees. The edges were considered sharp, thus neglecting the effects of wear and manufacturing processes, which, as discussed before, produce a certain radius on the edges. Although the aim of that paper is different from the aim of this paper, that paper [8] proves that it is possible to simulate the fluid flow through the clearance between a spool and its bushing sleeve, provided that a sufficiently fine mesh is generated in the narrow fluid zone.
In [9], the effects of different radii on the spool edge of a commercially available servovalve were analyzed using a partial three-dimensional model solved by Ansys Fluent. The analysis assumed that the clearance between the spool and bushing sleeve was zero and that the edge of the bushing sleeve was sharp. The numerical predictions show that, as expected, the increase in the radius on the spool edge increases the internal leakage at null. There are other papers in the scientific literature that have tried to predict the erosion rate of the metering edges in servovalves caused by contamination particles, using both analytical approaches and CFD analyses [10-13]. However, these investigations have mainly been carried out for opening degrees far from the null position.
The research presented in this paper aims at predicting the effects of round edges on the spool and bushing sleeve as well as clearances, upon the internal leakage around null in the main stages of servovalves. To this end, accurate 2D computational fluid dynamic (CFD) models are used. The main feature of this analysis is that the numerical results are generic, since they are applicable to any servovalve. This analysis can be useful for manufacturers, since it allows prediction of the leakage around null for a wide range of edge radii, clearances and overlaps. This analysis has been carried out as a collaboration among the University of Bath, the Polytechnic University of Bari, and Moog Controls Ltd, a world leading manufacturer of servovalves.

CFD MODELS

This section describes the models and computational domains used to carry out the investigation on the internal leakage.
The first domain considered is that reproducing a part of an existing Moog valve. A sketch of this domain is shown on the left of Fig.1, which also shows the boundary zones used.

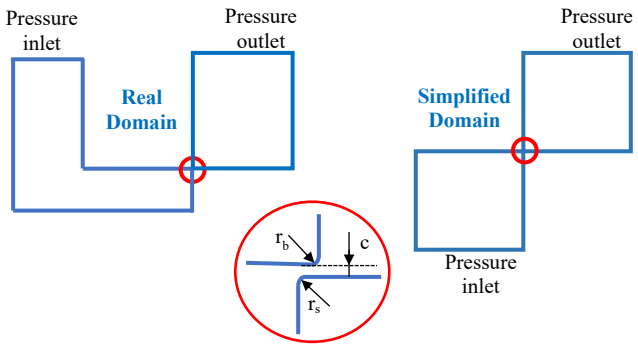

Fig.1. Domain reproducing a part of an existing Moog's valve (left) and simplified domain (right), r_b=bushing radius, r_s= spool radius, c=clearance.

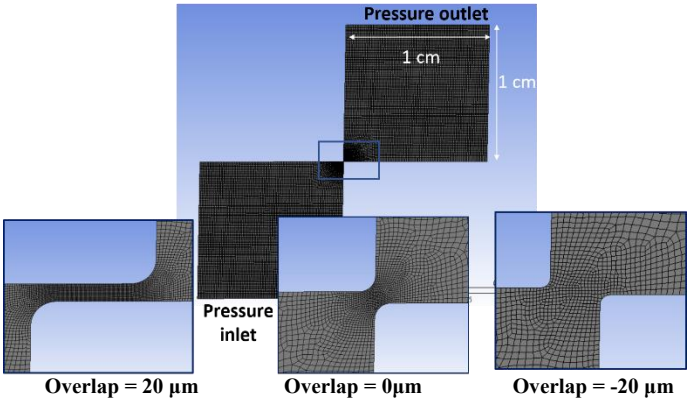

Fig.2 Computational mesh for the simplified 2D model and enlargement on the narrow flow passage: overlap = 20 µm (left), overlap = 0 µm (centre), overlap = -20 µm (right).

The second domain considered is shown on the right of Fig.1: it is a simplified domain having all the edges with the same length. The boundary conditions are the same for the two domains, namely, pressure inlet was set at the inlet edge and pressure outlet was set at the outlet edge. All the other edges present in the domains were defined as walls.

The two domains were meshed with the same strategy resulting from a grid convergence analysis, not reported here for brevity, in which the monitored parameter was the flow rate. Specifically, the elements in the restriction were meshed with a dimension of 0.1 µm; the maximum size of the edges of the elements was taken equal to 0.1 mm (far from the restriction), and the growing rate was 1.05. The computational mesh for the simplified 2D domain is shown in Fig. 2. The overall mesh size slightly changed according to the geometrical features (overlap, clearance and radius), ranging from 22000 to 30000 cells.

In addition to the two domains, two different settings have been considered to solve the Reynolds Averaged Navier-Stokes (RANS) equations in Ansys Fluent. The first one is an incompressible single-phase model, in which the oil is treated as a fluid with constant density ρ and dynamic viscosity μ. The values considered for the density and viscosity are the same as those of Hyjet at 40 °C, namely ρ=985 kg/m^3 and μ=0.01 kg/(ms).

The second one is an incompressible two-phase (mixture) model capable of taking into account the occurrence of cavitation. The primary phase is again oil treated as incompressible fluid (namely, Hyjet at 40 °C, with ρ=985 kg/m^3 and μ=0.01 kg/(ms)). Instead, the secondary phase is incompressible vapor oil with ρ=4 kg/m^3 and μ=3·10^{-6} kg/(ms), generated when the local pressure decreases down to the vaporization pressure. Fluent provides three cavitation models: the Schnerr-Sauer model, the Zwart-Gerber-Belamri model and the Singhal et al. model [14]. Previous experiences showed that the Schnerr-Sauer model is very robust while providing accurate predictions of the cavitation phenomenon [15]. For these reasons, it was selected for this simulation work. This model is not capable of taking into account the presence of non-condensable gases in the liquid, which can change the density of the vapor cavities. Preliminary investigations have shown that, in terms of flow rate, the results will not substantially change by considering different properties for the vapor oil due to the interaction with the dissolved gases. For example, using the vapor properties equal to those of air at atmospheric pressure, namely, ρ=1.225 kg/m^3 and μ=1.7894e^{-05} kg/(ms), leads to negligible differences in terms of flow rate.

As far as turbulence is concerned, it was predicted using the *RNG K-ε* model with the enhanced wall treatment. This model for the prediction of turbulence has proved to be very effective in the case of a flow field through a restriction, as occurs in hydraulic valves [15-18]. It also provides very accurate results for a wide range of the Reynolds number, even for transitional flows [15-18]. As successfully done in previous modelling works of proportional valves [15-18], the best strategy associated with the enhanced wall treatment consists in meshing the domain across the restrictions with a high number of cells, while the domain far from the restrictions can be discretized with a coarser mesh. This can allow the high gradients of velocity across the restrictions to be accurately simulated while maintaining a reasonable computational time.

With regard to the discretization of the equations, the second order upwind method was selected for momentum, turbulent kinetic energy and turbulent dissipation rate equations. The selected pressure interpolation scheme is second order accurate for the single-phase model, while the PREssure STaggering Option (PRESTO) was selected for the mixture (cavitation) model.

With both the single-phase and the mixture model, 2000 iterations were enough to reach converged values for the flow rate, with all the scaled residuals being below 10^{-4}.

RESULTS

This section reports the results achieved with the fluid computational domains and numerical models described in the previous section. In particular, at first the comparison between the real domain and the simplified one is discussed, to show that the simplified domain can effectively be used to predict the internal leakage for any servovalve. Then, the numerical models (both the single-phase model and the two-phase one) are validated by comparison with available experimental data. Subsequently, the numerical models are used to obtain some useful charts for fixed values of the pressure drop, showing how the internal leakage changes as a function of the overlap, clearance and radius on the edges of the both the spool and bushing sleeve. Finally, some analytical correlations are given to evaluate the internal leakage for different values of the pressure drops.

Comparison between the simplified 2D domain and the real domain.

In this subsection, the simplified 2D domain is compared with the real domain reproducing a part of an existing valve (see Fig.1). In this comparison, the two domains have the same geometry as far as the restricted section is concerned, namely,

radius on the edges of the spool and bushing sleeve equal to 4 μm (r_b=r_s=4 μm), clearance between the spool and bushing sleeve equal to 3 μm (c=3 μm) and zero overlap between spool edge and bushing sleeve edge (overlap=0 μm).
The comparison was performed by setting an inlet pressure equal to 70 bar, an outlet pressure equal to 1 bar, and by using the single-phase model. The choice of 70 bar for the pressure inlet stems from the fact that this value of inlet pressure is usually employed in the null tests of servovalves.
The contours of the predicted pressure for the real domain are reported in Fig. 3. It is noteworthy that the pressure drop is mainly located across the restriction, and all the remaining fluid domain does not experience appreciable pressure variations.

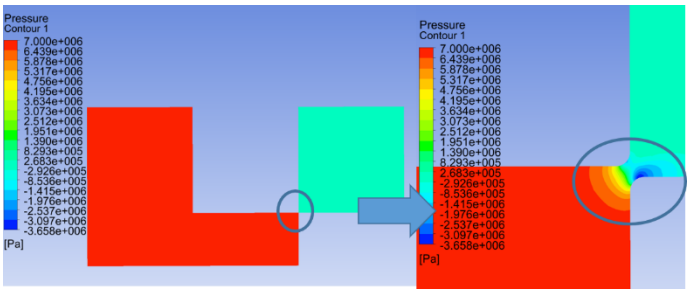

Fig.3. Contours of pressure predicted for the real domain (pressure inlet=70 bar, pressure outlet=1 bar, single-phase model, radius on the edges=4 μm, clearance=3 μm, overlap=0 μm)

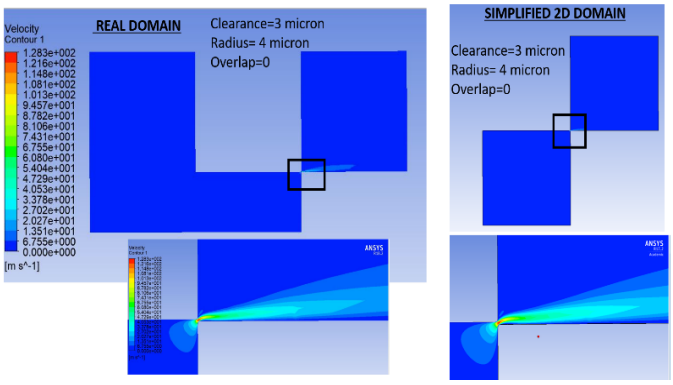

Fig.4. Contours of velocity predicted for the real domain (left) and for the simplified domain (right) (pressure inlet =70 bar, pressure outlet=1 bar, single-phase model)

Fig.4 shows the comparison, in terms of velocity contours, between the real domain and the simplified one. It is noteworthy that the contours are very similar in the two cases; even the predicted flow rate is the same, namely, Q = 0.0335 l/(min mm). The two case studies have produced the same results because the pressure drop is mainly located across the restriction, as shown in Fig. 3. This suggests that, for this specific analysis of the internal leakage, there is no need to simulate the entire flow field inside a real valve, but it is sufficient to simulate the flow field across the metering section with a simple 2D domain. This also suggests that the results obtained with such a simplified 2D model have general validity and can be applied to different valves.

Validation of the 2D simplified model

The previous section has highlighted that, because the pressure drop is mainly located across the restriction, a simplified 2D model can be used to predict the internal leakage, and the results obtained will have general validity. With this 2D modelling, the direct leakage flow can be predicted in a plane. To obtain the overall direct leakage flow, the predicted flow value must be multiplied by the slot width and the number of slots.
The contours of pressure in Fig. 3 show that the single-phase model predicted negative pressure values inside the restriction. Since this is not physically possible, it can be deduced that cavitation occurs in the restriction, thus demanding for the cavitation model described earlier, in order to properly predict the formation of the cavitation cavities.
This section compares some available experimental data with the numerical predictions of the 2D simplified domain resolved with both the single-phase model and the cavitation model. Specifically, the experimental data used in this analysis to validate the numerical models were retrieved from the null plot of an existing Moog valve. The null plot is the plot of the flow rate (i.e., leakage flow rate) measured as a function of the spool position, for all the metering lands of a given spool coupled with its bushing sleeve. Fig.5 shows the null plot retrieved by Moog for a four-way three-position (4/3) Moog servovalve. Because it is a 4/3 valve, four flow rate curves are present in the null plot, as many as the four metering lands of the spool. These curves are usually not plotted for very low values of the flow rate, because of the large measurement errors associated with these conditions (i.e., for very small spool positions and flow rates).

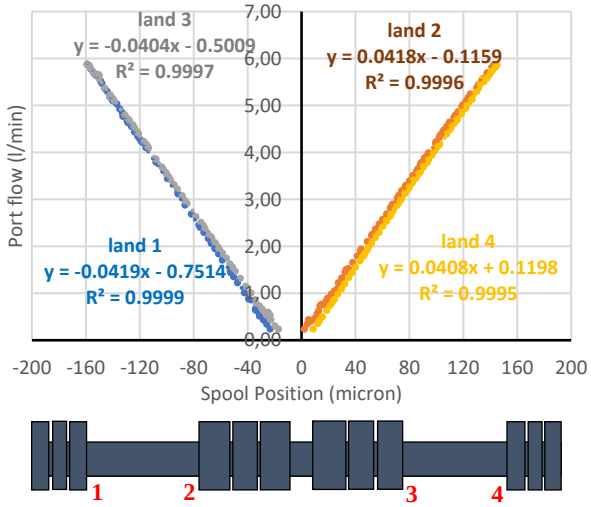

Fig.5. Null plot for an existing Moog valve used for the experimental validation of the numerical models

What can be used from this graph to validate the numerical models is the average slope of the four flow rate curves. The average slope in the underlap region is not affected by uncertainties related to the edge radius, clearance and eccentricity. The same strategy to validate the numerical model was adopted in [9], although the authors of that paper neglected the clearance and radius on the bushing sleeve in their CFD model, as previously discussed.

The value of the clearance is known for the valve tested in the null test, which is c=3 µm. Geometrical data regarding the roundness of the edges are not available. The maximum error associated with the flow meter was ± 0.08 l/min. The same inlet pressure as that of the experimental tests was used in the simulation to allow the comparison, namely, pressure inlet= 70 bar. During the test, the outlet pressure was of the order of 1 bar. This value was set as the outlet pressure in the simulations. The oil used in the null tests was Hyjet at 40 °C, with ρ=985 kg/m^3 and μ=0.01 kg/(ms). The same fluid conditions were used in the simulations.

To allow the comparison, the numerical curves were obtained by multiplying the flow rate predicted in the plane by the slot width (4.07 mm) and number of slots (2 per land) of the tested valve.

Because the radius on the spool and bushing sleeve edge was not measured in the experimental tests, different radii were considered in the simulations. Fig. 6 shows the flow rates predicted by the single-phase model for underlap conditions (namely, overlap < 0) and for a wide range of radii on the edges (assumed equal on the bushing sleeve and spool). This range for the radius (from 2 micron to 10 micron) is the expected range for a common servovalve, according to Moog's database. As visible in this graph, the slopes of the five numerical curves are very similar (the maximum percentage difference among these is 2.8%). Therefore, the main effect of the radius increase in the underlap zone is to increase the y-intercept.

Fig. 7 compares the single-phase model curve and the cavitation model curve in the underlap and overlap regions, for a selected radius of 4 µm (as shown in Fig. 6, a different radius will have a very similar slope in the underlap region). The two numerical curves are compared with the dashed curve, which has the same slope as the average slope retrieved from the null plot.

It is noteworthy that the error between the slope of the cavitation curve in the underlap region and the experimental slope is only 3%. This shows that the CFD model is highly accurate and that cavitation occurred during the experimental test.

The difference in terms of slope between the "cavitation" curve and the "single-phase" one is about 9%. However, the effects of cavitation in terms of flow rate are negligible in the zone of interest (namely, in the overlap region for overlaps less than 10 µm, which is the most common situation for servovalves). Moreover, a very similar slope between the experimental data and the numerical predictions suggests that the circumferential leakage (neglected in this analysis) will not much change the slope of the curves.

Figure 8 shows the qualitative results obtained with the cavitation model for an overlap of 20 µm (left) and for an overlap of -20 µm (right), with inlet pressure=70 bar, outlet pressure=1 bar, clearance =3 µm, and radius=4 µm. The pictures in Fig.8 show the pressure, vapour fraction and velocity vectors predicted with the cavitation model. It is notable that the negative pressures have disappeared compared to Fig. 3, and that the cavitation cavities are mainly located in the recirculation zones just downstream of the restriction. As a confirmation of the results of Fig. 7, the contours of vapour fraction (Fig. 8b) show that the effects of cavitation are negligible in the overlap conditions, whereas they become more important in the underlap region.

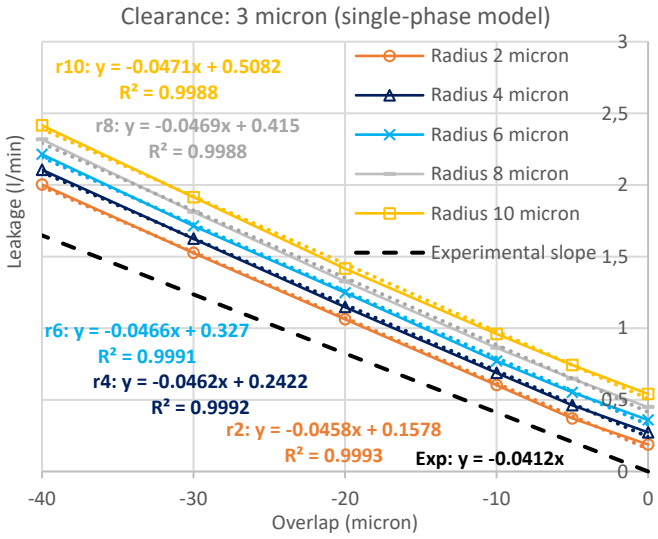

Fig.6. Comparison among the numerical predictions of the single-phase model for different radii and the average experimental slope of the null plot in the underlap region (inlet pressure=70 bar, outlet pressure=1 bar, clearance =3µm).

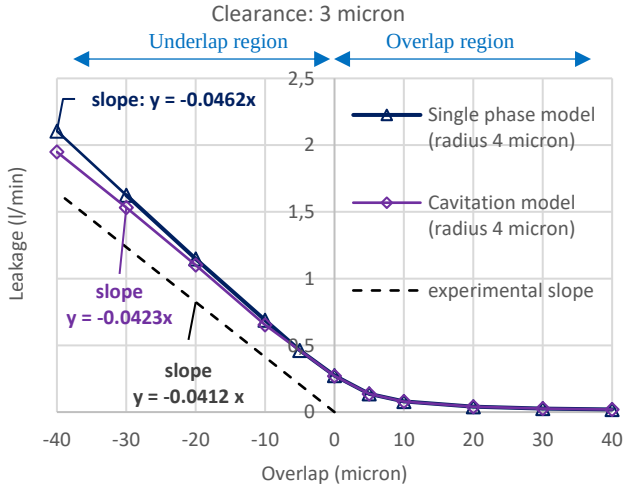

Fig.7. Comparison among the single-phase model, cavitation model, and the average slope of the null plot (inlet pressure=70 bar, outlet pressure=1 bar, clearance =3µm).

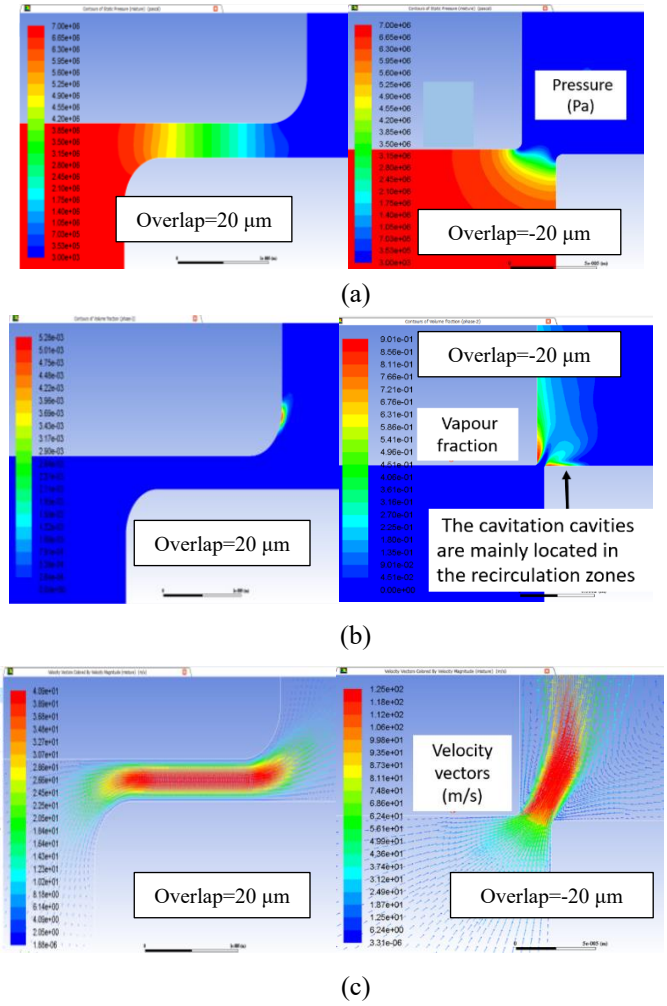

Fig.8. Contours of pressure (a), vapour fraction (b) and velocity vectors (c), predicted by the cavitation model in the simplified domain (inlet pressure=70 bar, outlet pressure=1 bar, clearance =3µm, radius=4µm), for overlap=20 µm (left) and overlap=-20 µm (right).

<u>Results for the direct leakage flow as a function of the clearance and edge radius.</u>

Since the effects of cavitation, as far as the magnitude of the flow rate is concerned, are negligible in the zone of interest, the single-phase model applied to the simplified 2D domain (see Fig.2) was used to obtain graphs of the direct leakage flow as a function of the clearance and radius on the edges (assumed equal for the bushing sleeve and the spool). The overlap was varied from -40 µm to 40 µm, with the negative values indicating an underlap condition. Although the most common situation in servovalves is that with overlaps comprised between 4 µm and 7 µm, a wider range of overlaps and underlaps has been considered, in order to provide generic results which can also be applied to other types of spool valves, such as proportional valves [16]. It must be noted that, according to the previous comparison between the single-phase model and the cavitation one (see Fig. 7), these graphs, obtained with the single-phase model, will overpredict the direct leakage flow by about 9% for large values of the underlap.

The outlet pressure was set to 1 bar, and three values for the inlet pressure were considered, namely 70 bar (Fig. 9), 110 bar (Fig.10) and 150 bar (Fig. 11). For each pressure drop, four graphs were obtained, as many as the values considered for the clearance, namely, 3 µm (a), 4 µm (b), 6 µm (c), and 8 µm (d). These graphs can be applied to both the high-pressure chamber and the low-pressure chamber of a 4/3 valve, provided that the pressure drop is the same.

These graphs (Fig. 9-11) provide the direct leakage flow in a plane. The overall direct leakage flow can be obtained by multiplying the predicted value and the slot widths and number of slots of a given valve. The value obtained must be increased by a certain amount to account for the circumferential leakage. The contribution of the circumferential leakage will be evaluated in forthcoming studies.

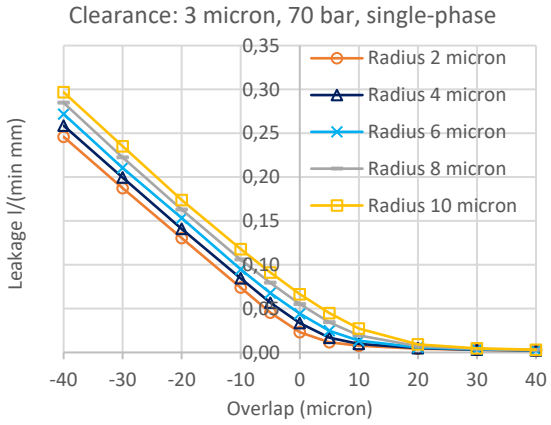

(a)

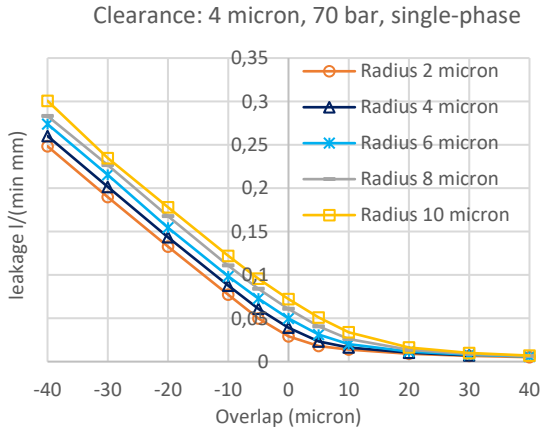

(b)

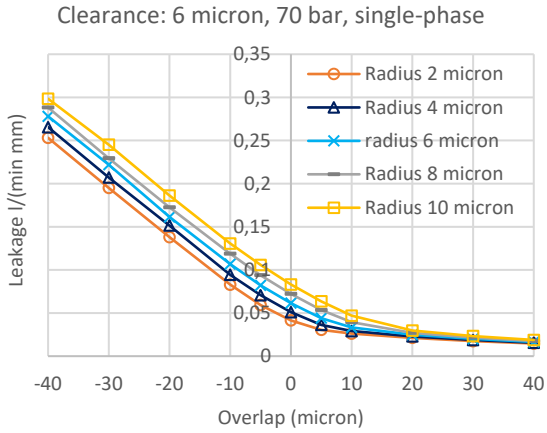

(c)

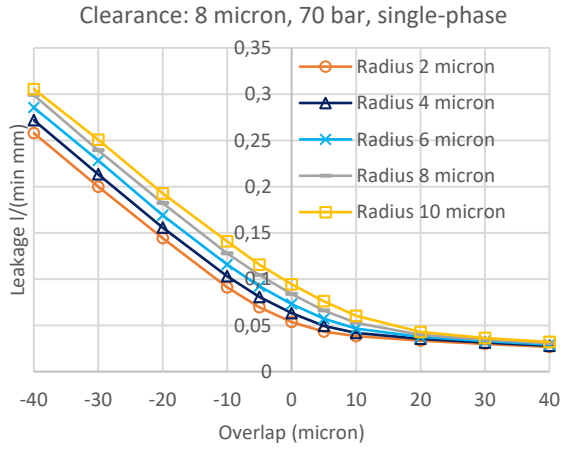

(d)

Fig.9. Prediction, by using the single-phase model, of the direct leakage flow for an inlet pressure of 70 bar and an outlet pressure of 1 bar: clearance c=3 μm (a), c=4 μm (b), c=6 μm (c), c=8 μm (d).

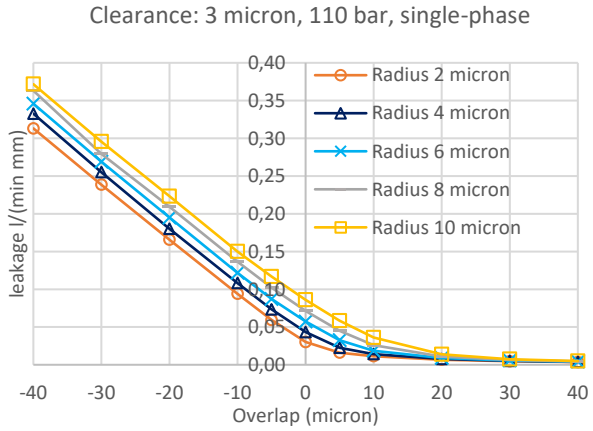

(a)

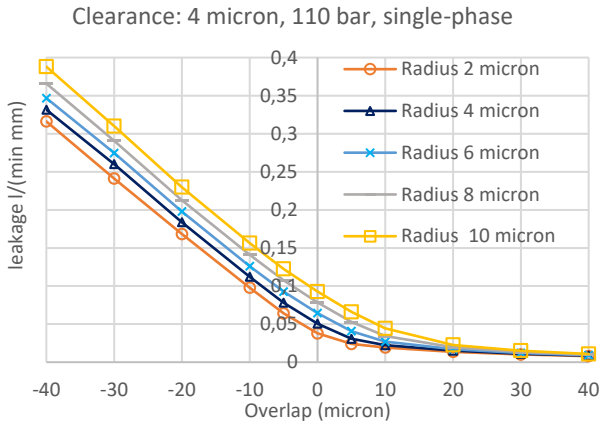

(b)

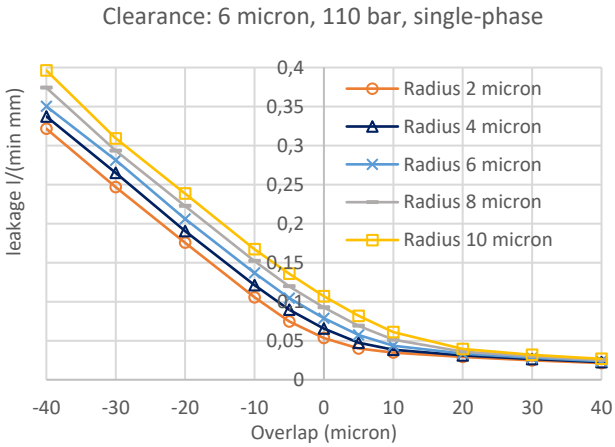

(c)

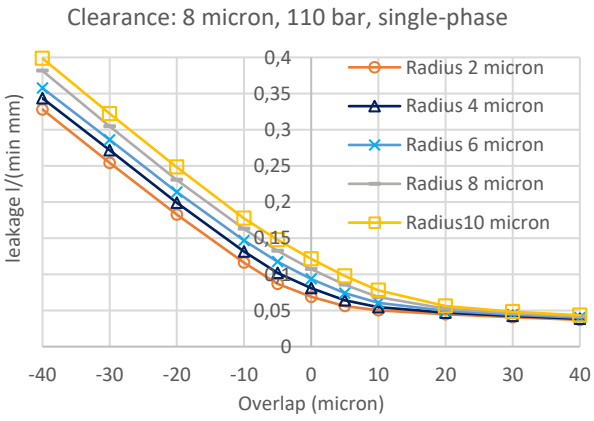

(d)

Fig.10. Prediction, by using the single-phase model, of the direct leakage flow for an inlet pressure of 110 bar and an outlet pressure of 1 bar: clearance c=3 μm (a), c=4 μm (b), c=6 μm (c), c=8 μm (d).

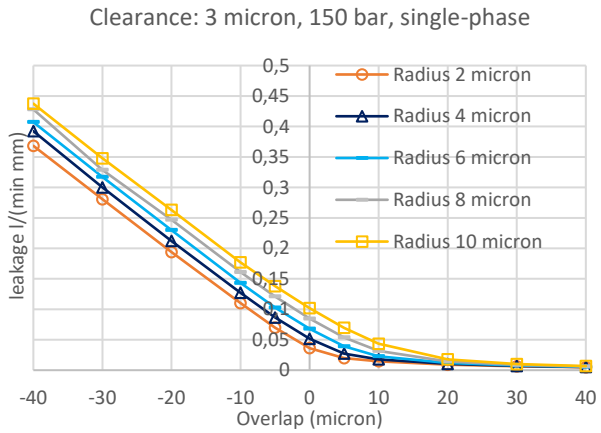

(a)

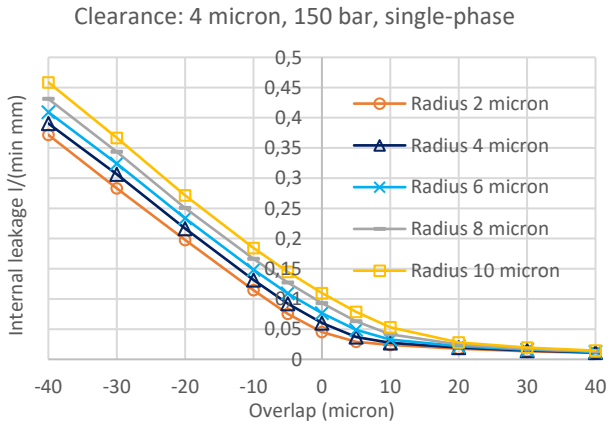

(b)

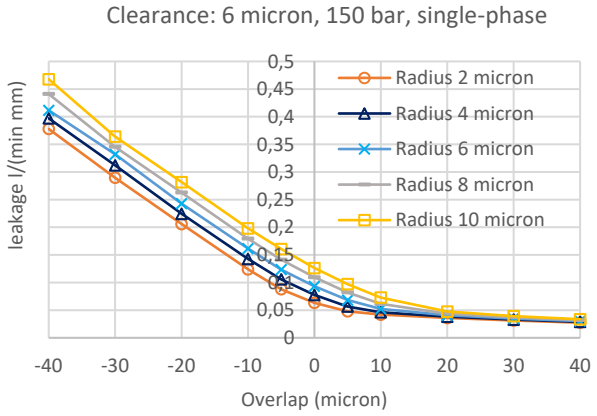

(c)

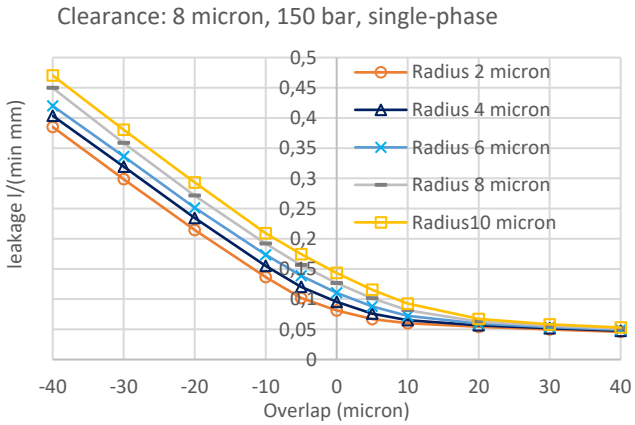

(d)

Fig.11. Prediction, by using the single-phase model, of the direct leakage flow for an inlet pressure of 150 bar and an outlet pressure of 1 bar: clearance c=3 μm (a), c=4 μm (b), c=6 μm (c), c=8 μm (d).

The graphs show that both the clearance and the radius have a huge effect on the internal leakage, therefore it is important to limit their values as much as possible during the manufacturing processes if the aim is to reduce the power consumption. It is also visible that the overlap condition between the spool and the bushing sleeve has a huge impact on the leakage flow. For given values of radius and clearance, the presence of some degree of overlap between the spool land and the bushing sleeve port width can help to reduce the leakage flow at null.

In the previous graphs, an equal radius on the spool edge and on the bushing sleeve edge was assumed. However, if the radius on the spool edge is different from the radius on the bushing edge, the previous graphs can still be used by taking an equivalent radius equal to the average of the two radii.

As a confirmation of this, the graph in Fig. 12 compares: the leakage flow obtained for a radius on the spool equal to 2 μm and a radius on the bushing equal to 10 μm (blue dots), and the leakage flow obtained for a radius on the spool equal to 6 μm and a radius on the bushing equal to 6 μm (grey line). The red curve is the plot of the percentage difference between the two cases. This graph was obtained by using the single-phase model, for an inlet pressure of 70 bar and an outlet pressure of 1 bar (clearance c=3 μm). As shown by the graph, the difference between the two cases is negligible, being always below 5%.

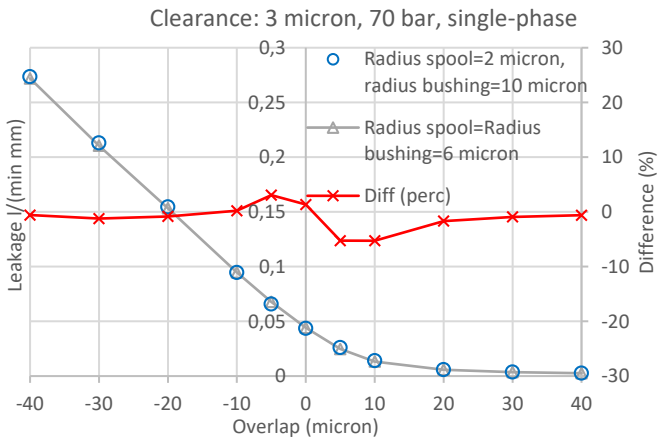

Fig.12. Comparison between the leakage flow obtained for r_b= r_s =6 μm (grey line), and the leakage flow obtained for r_b=10 μm and r_s =2 μm (blue dots), by using the single-phase model, for an inlet pressure of 70 bar and an outlet pressure of 1 bar (clearance c=3 μm).

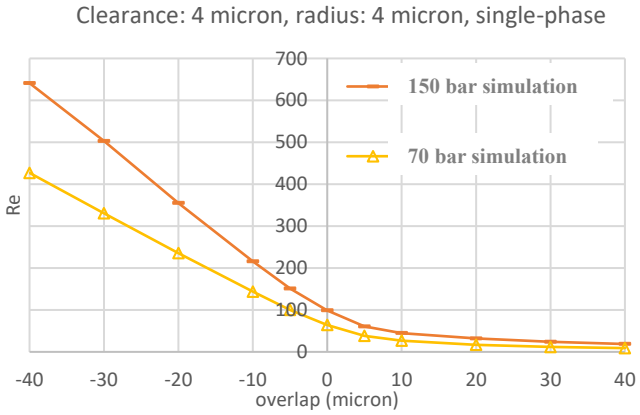

Fig.13. Reynolds number calculated through equation 2 using the flow rate predicted by the single-phase model for 70 bar inlet pressure and 150 bar inlet pressure.

Calculation of the internal leakage for different pressure drops

The graphs shown in the previous sub-section can allow the direct leakage flow to be estimated for a fixed pressure drop (inlet pressure = 70 bar, 110 bar or 150 bar, and outlet pressure =1 bar). For a different pressure drop, two different strategies can be attempted.

The first one, which is the more accurate, consists in running the simulations again with the new value of the pressure drop.

The second one consists in using some analytical formulas along with the available data retrieved from the above graphs. The analytical formulae available in the literature depend on the fluid regime, namely laminar or turbulent flow [3]. In the present study, there is a large variation of the Reynolds number Re, which can be calculated as follows:

$$Re = \frac{\rho V l}{\mu} = \frac{\rho Q}{\mu} \qquad (2)$$

where V is the average velocity in the restriction having a characteristic length l, and Q is the flow rate predicted in the plane. As a confirmation of this, Fig. 13 shows that the Reynolds number, calculated for the 70 bar curve and for the 150 bar curve with a clearance of 4 μm and a radius of 4 μm, changes significantly depending on the overlap and the pressure drop. According to Merritt [3], the transitional Reynolds number for a sharp orifice can range from about 9 to about 400 depending on the type of orifice; however, a precise value for the transitional Reynolds number is not available for the present case.

Depending on the fluid regime, either equation (3) or equation (4) could be used [3]:

$$\frac{\bar{Q}}{Q} = \sqrt{\frac{\overline{\Delta p}}{\Delta p}} \qquad (3)$$

$$\frac{\bar{Q}}{Q} = \frac{\overline{\Delta p}}{\Delta p} \qquad (4)$$

In equations (3) and (4), Q is the value of flow rate (leakage flow) retrieved from the graphs of Fig. 9-11 for a given value of the pressure drop Δp (namely, inlet pressure = 70 bar, 110 bar or 150 bar, and outlet pressure =1 bar); instead, $\bar{Q}$ is the new value of flow rate for a different value of the pressure drop $\overline{\Delta p}$. Equation (3) assumes that the flow is turbulent (namely, the flow rate is proportional to the square root of the pressure drop), instead equation (4) assumes that the flow is laminar (namely, the flow rate is proportional to the pressure drop) [3].

Fig.14 (a) shows the flow rate predicted by the simulations for an inlet pressure of 70 bar (yellow curve) and 150 bar (orange curve). In addition, Fig. 14 (a) shows the flow rate curve obtained through equation (3) from the simulated flow rate curve at 70 bar (blue curve). Fig. 14 (b) shows an enlargement of the graph of Fig.14 (a) in the underlap region. The graphs show that equation (3) can allow a good evaluation of the leakage flow both in the underlap region and in the overlap region for overlaps approximately lower than 20 μm. For overlaps ≥ 20 μm, equation (3) leads to large errors, greater than 20%. This can be due to the fact that for large values of the overlap, the flow becomes laminar, which is a condition inconsistent with equation (3).

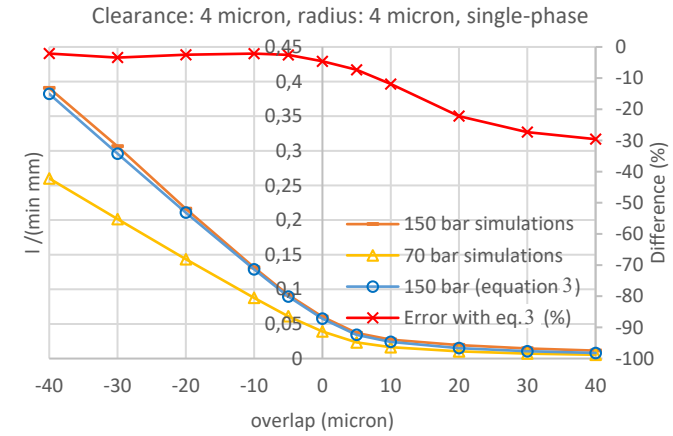

(a)

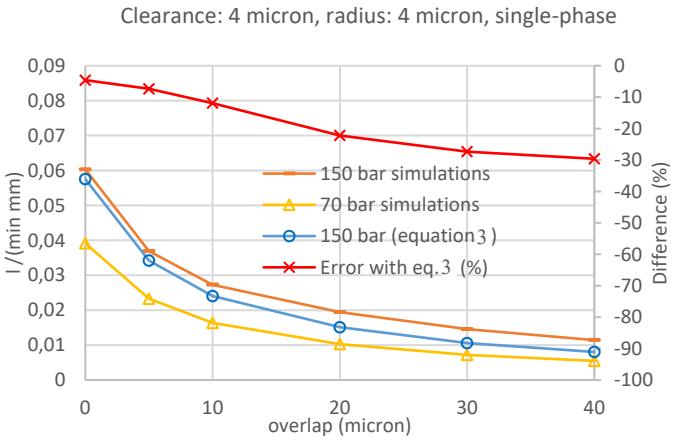

(b)

Fig.14. Flow rate predicted with the simulations for an inlet pressure of 70 bar (yellow curve) and 150 bar (orange curve), and flow rate obtained, through equation (3), from the simulated flow rate curve at 70 bar (blue curve); red curve: difference % between the blue curve and the orange one; Fig.14 (b) is an enlargement of Fig. 14 (a) in the overlap region. Results obtained for radius r_b=r_s=4 μm and clearance c=4 μm.

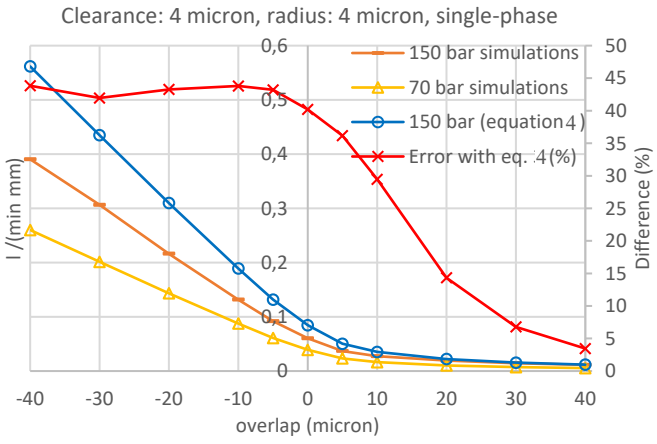

(a)

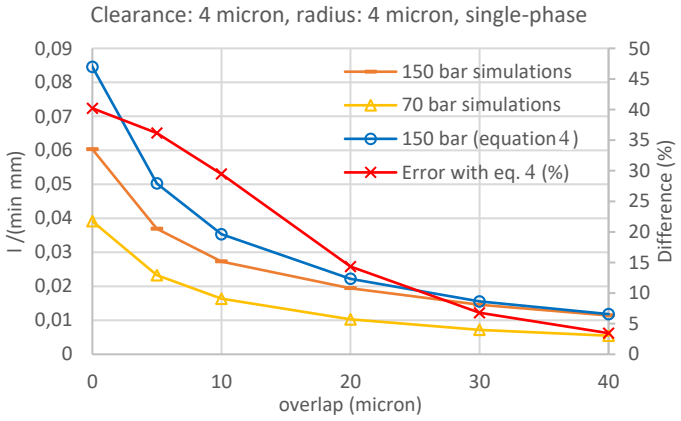

(b)

Fig.15. Flow rate predicted with the simulations for an inlet pressure of 70 bar (yellow curve) and 150 bar (orange curve), and flow rate obtained, through equation (4), from the simulated flow rate curve at 70 bar (blue curve); red curve: difference % between the blue curve and the orange one; Fig.15 (b) is an enlargement of Fig. 15 (a) in the overlap region. Results obtained for radius r_b=r_s=4 μm and clearance c=4 μm.

Instead, for large values of the overlap, equation (4) can be used. In this regard, the graph of Fig. 15 again shows the flow rate predicted by the simulations for an inlet pressure of 70 bar and 150 bar (yellow curve and orange curve, respectively). However, in this case, Fig. 15 shows the flow rate curve obtained through equation (4), instead of equation (3), from the simulated flow rate curve at 70 bar. It is noteworthy that equation (4) allows a good estimation of the leakage flow for high degrees of overlap, namely, for laminar flows, with the percentage error being lower than 15% for overlaps ≥ 20 μm. However, for low values of overlap and in the underlap region, equation (4) produces large errors, due to the fact that the flow ceases to be laminar. As a conclusion, it can be deduced that equation (3) and equation (4) can both be effectively used, but for different ranges of the overlap.

As a final consideration, the simulations performed to retrieve all the above graphs were obtained with the RNG k-ε model with the enhanced wall treatment to predict the turbulence. However, this final analysis has revealed that the flow can be assumed laminar for overlaps ≥ 20 μm. Nevertheless, as demonstrated in similar studies of the flow through restrictions [15, 17], the RNG k-ε model with the enhanced wall treatment can still be used in laminar conditions, providing very accurate results. In this regard, Table 1 compares the results in the laminar zone obtained with the RNG k-ε model and with the laminar model (both single-phase). It is shown that the numerical predictions are very similar, thus demonstrating the reliability of the RNG k-ε model for a wide range of Reynolds number.

Overlap (μm)	Flow rate with the RNG k-ε model l/(min mm)	Flow rate with the laminar model l/(min mm)
20	0.004929	0.004928
30	0.003239	0.003237
40	0.002409	0.002408

Table 1. comparison between the flow rate predicted by the RNG k-ε model with the enhanced wall treatment and the flow rate predicted by the laminar model for very high values of the overlap (radius=4 micron, clearance 3 micron, 70 bar inlet pressure, 1 bar outlet pressure, single-phase models).

CONCLUSIONS

This paper has analyzed, through a 2D CFD analysis, the effects of geometrical imperfections (i.e., radii on the spool edge and bushing sleeve) and tolerances (i.e., radial clearance and axial overlap between the spool and bushing sleeve) upon the internal leakage in the second stages of servovalves. The following conclusions can be drawn:

- the prediction of the direct leakage can be obtained using a simple 2D domain applicable to any valve;
- therefore, a 2D model has been realised, which is also capable of predicting cavitation;
- cavitation predicted by the model occurs in the low-pressure metering chamber. However, the effects in terms of flow rate are negligible for overlap conditions (the most common situation in servovalves);
- the model realized is very accurate, as demonstrated by comparison with experimental data;
- several graphs have been obtained (for inlet pressure = 70 bar, 110 bar and 150 bar, and outlet pressure =1 bar), showing the direct leakage flow predicted on a plane as a function of the overlap, clearance and edge radius. The overall direct leakage in a real spool valve can be obtained by multiplying the predicted value by the overall slot width;
- if the radius on the spool edge is different from the radius on the bushing edge, the graphs can still be used by taking an equivalent radius equal to the average of the two radii;
- for different values of the pressure drop, some analytical correlations can be used to evaluate the direct leakage flow from the data taken from the graphs provided.

Forthcoming work will be focused on assessing the effects of the circumferential leakage upon the overall leakage flow for slotted spools. To this end, 3D CFD simulations of the circumferential path will be carried out for a wide range of geometrical parameters. The predicted percentage increase due to the circumferential leakage will be used to correct the direct leakage obtained from the graphs analyzed in this paper.

REFERENCES

1. Tamburrano, P., Plummer, A. R., Distaso, E., & Amirante, R. (2018). A review of electro-hydraulic servovalve research and development. International Journal of Fluid Power, 1-23.
2. Plummer, A.R. “Electrohydraulic servovalves – past, present, and future,” 10th Int. Fluid Power Conf., pp. 405–424, 2016.
3. Merritt, Herbert, Herbert E. Merritt, and Herbert E. Merritt. Hydraulic control systems. John Wiley & Sons, 1967.
4. Ellman A. Leakage behaviour of four-way servovalve, Proceedings of the ASME Fluid Power Systems and Technology, Vol. 5, 1998, pp. 163–167.
5. Gordić, D., M. Babić, D. Milovanović, and S. Savić. "Spool valve leakage behaviour." Archives of Civil and Mechanical Engineering 11, no. 4 (2011): 859-866.
6. Eryilmaz, Bora, and Bruce H. Wilson. "Modeling the internal leakage of hydraulic servovalves." In International Mechanical Engineering Congress and Exposition, ASME, vol. 69, pp. 337-343, 2000.
7. Eryilmaz, Bora, and Bruce H. Wilson. "Combining leakage and orifice flows in a hydraulic servovalve model." Journal Of Dynamic Systems Measurement And Control 122, no. 3 (2000): 576-579.
8. Di Rito, Gianpietro. "Experiments and CFD simulations for the characterisation of the orifice flow in a four-way servovalve." International Journal of Fluid Power 8, no. 2 (2007): 37-46.
9. Pan, Xu Dong, Guang Lin Wang, and L. Zhang. "Simulation study on spool edge’s round angle effects on spool valve orifice discharge characteristic." In Applied Mechanics and Materials, vol. 10, pp. 918-922. Trans Tech Publications, 2008
10. Zhang, Kun, Jinyong Yao, Tongmin Jiang, Xizhong Yin, and Xiaobo Yu. "Degradation behavior analysis of electro-hydraulic servo valve under erosion wear." In Prognostics and Health Management (PHM), 2013 IEEE Conference on, pp. 1-7. IEEE, 2013.
11. Zhang, Kun, Jinyong Yao, and Tongmin Jiang. "Degradation assessment and life prediction of electro-hydraulic servo valve under erosion wear." Engineering failure analysis 36 (2014): 284-300.
12. Yaobao, Yin, Yuan Jiayang, and Guo Shengrong. "Numerical study of solid particle erosion in hydraulic spool valves." Wear 392 (2017): 174-189.
13. N.D. Vaughan, P.E. Pomeroy, D.G. Tilley, The contribution of erosive wear to the performance degradation of sliding spool servovalves, Proc. Inst. Mech. Eng. Part J: J. Eng. Tribol. 212 (6) (1998) 437–451.
14. ANSYS FLUENT Theory Guide 14.0. November 2011. Fluent Inc.
15. Amirante, R., Distaso, E., & Tamburrano, P. (2014). Experimental and numerical analysis of cavitation in

hydraulic proportional directional valves. Energy Conversion and Management, 87, 208-219.
16. Tamburrano, P., Plummer, A. R., Distaso, E., & Amirante, R. (2019). A review of direct drive proportional electrohydraulic spool valves: industrial state-of-the-art and research advancements. Journal of Dynamic Systems, Measurement, and Control, 141(2), 020801.
17. Amirante, R., Catalano, L. A., Poloni, C., & Tamburrano, P. (2014). Fluid-dynamic design optimization of hydraulic proportional directional valves. Engineering Optimization, 46(10), 1295-1314.
18. Amirante, R., Distaso, E., & Tamburrano, P. (2016). Sliding spool design for reducing the actuation forces in direct operated proportional directional valves: Experimental validation. Energy Conversion and Management, 119, 399-410.